Deep Structure of Subducting Slabs and Mantle Plumes from Global Tomography

Tôhoku Geophys. Journ. (Sci. Rep. Tôhoku Univ., Ser. 5), Vol. 36, No. 2, pp. 111-130, 2001

Deep Structure of Subducting Slabs and Mantle Plumes from Global Tomography

DAPENG ZHAO

Geodynamics Research Center, Ehime University, Matsuyama 790-8577, Japan
(e-mail: zhao@sci.ehime-u.ac.jp)

(Received November 14, 2000; accepted January 9, 2001)

Abstract: In order to better understand the deep structure and dynamics of the Earth's interior, we have attempted to develop a new model of whole mantle seismic tomography with a novel approach. We adopted a grid parameterization instead of blocks which were used in most of the global tomographic studies. Ray paths and travel times are computed with an efficient 3-D ray tracing scheme. Moreover, the topography of mantle discontinuities at 410 and 660 km depths are taken into account in the tomographic inversions. This new approach was applied to a large data set of ISC travel times (P, PP, PcP, pP) to determine a whole mantle P-wave tomography. For the shallow mantle, our new model contains the general features observed in the previous models: a low-velocity ring around the Pacific Ocean basins and high-velocity anomalies under the old and stable continents in the depth range of 0-400 km. One significant difference from the previous models is that stronger and wider high-velocity anomalies are visible in the transition zone depths under the subduction zone regions, which suggests that most of the slab materials are stagnant for a long time in the transition zone before finally dropping down to the lower mantle. Plume-like slow anomalies are visible under the hotspot regions in most parts of the mantle. The slow anomalies under hotspots usually do not show a straight pillar shape, but exhibit winding images, which suggests that plumes are not fixed in the mantle but can be deflected by the mantle winds. As a consequence, hotspots are not really fixed but can wander on the Earth's surface, as evidenced by the recent geomagnetic and numeric modeling studies. Wider and more prominent slow anomalies are visible at the core-mantle boundary (CMB) than most of the lower mantle, and there is a good correlation between the distribution of slow anomalies at the CMB and that of hotspots on the surface, which suggest that most of the mantle plumes under the hotspots may originate from the CMB. However, there may be some small-scaled, weak plumes originating from the transition zone depths.

1. Introduction

During the last two decades, seismologists have made continuous efforts to determine the three-dimensional (3-D) seismic velocity structure of the mantle (e.g., Dziewonski *et al.*, 1977; Nakanishi and Anderson, 1982; Dziewonski, 1984; Woodhouse and Dziewonski, 1984; Tanimoto, 1990; Inoue *et al.*, 1990; Zhang and Tanimoto, 1993; Su *et al.*, 1994; Vasco *et al.*, 1995; Zhou, 1996; Bijwaard *et al.*, 1998; Boschi and Dziewonski, 1999). These studies have greatly improved our understanding of the structure and dynamics of the Earth's deep interior.

In the present work, we propose a new 3-D P-wave velocity model of the mantle. This model has the following three distinct features from the previous models. First, we have taken into account the topography of mantle discontinuities in the tomographic

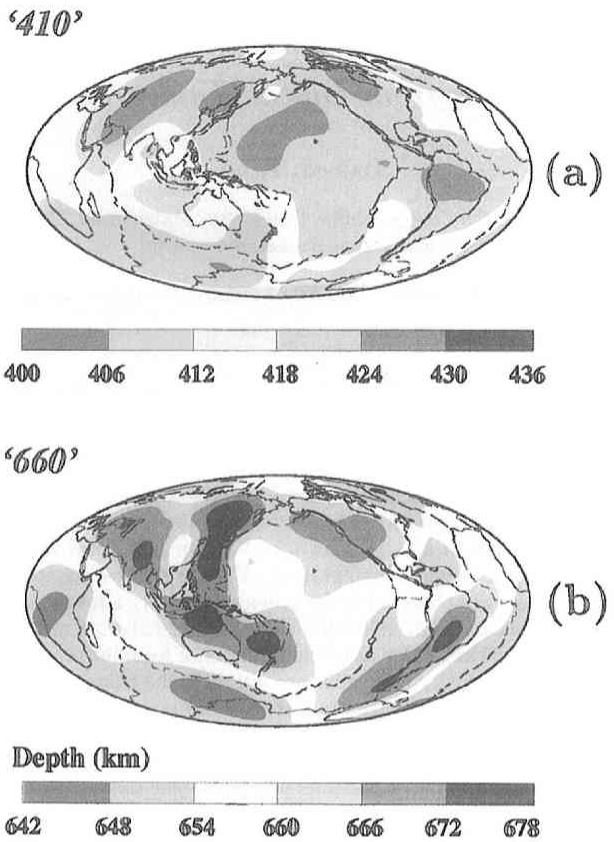

Fig. 1. Depth distribution of the (a) 410 and (b) 660 km discontinuities determined by Flanagan and Shearer (1998). The depth scale is shown below each of the maps.

inversions. It has been well established that several seismic velocity discontinuities exist in the mantle, such as the Moho discontinuity that separates the crust and mantle, and 410 km and 660 km discontinuities in the mantle transition zone (Dziewonski and Anderson, 1981 ; Kennett and Engdahl, 1991 ; Kennett *et al.*, 1995). Recently, Mooney *et al.* (1998) compiled the findings of seismic explosion studies conducted so far in the world and constructed a global map of the crustal thickness. Their results show that the Moho depth ranges from about 10 km under oceans to 40–70 km under the continents. Flanagan and Shearer (1998) used reflected waves to map the depth variations of the 410 and 660 km discontinuities (Figure 1). They found that the two discontinuities exhibit depth variations of up to 36 km. Such large depth changes of the three discontinuities would greatly affect the travel times and ray paths of seismic waves, and hence their topography should be taken into account in the tomographic inversions.

Local and regional scale tomographic studies have recognized the influences of the depth variations of seismic discontinuities, such as the Moho and the subducting slab

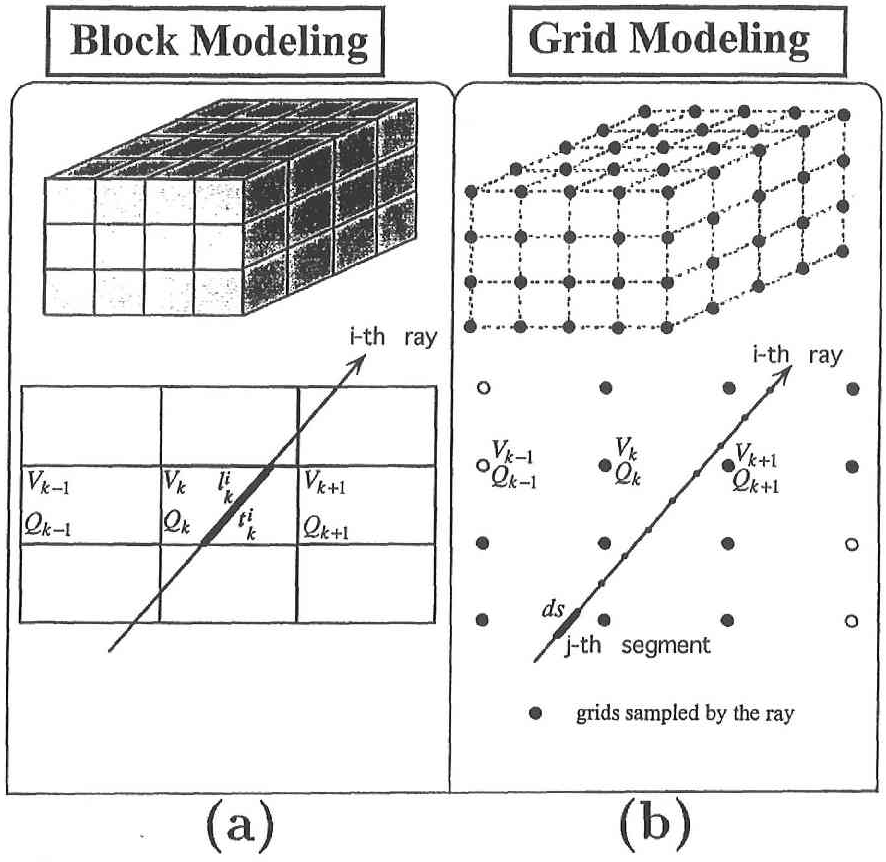

Fig. 2. A comparison of the (a) block and (b) grid parameterization to express the Earth structure. In the block approach, the velocity within each block is assumed to be constant, and the velocity changes abruptly across the boundaries between the blocks. Thus artificial velocity boundaries are introduced into the model in the horizontal and vertical directions between blocks. In the grid approach, velocity perturbations at the grid nodes are taken to be unknown parameters; the velocity perturbation at any point in the model is computed by linearly interpolating the velocity perturbations at the 8 grid nodes surrounding that point. Thus in the grid approach there is no artificial velocity discontinuity in the model.

boundary (Zhao *et al.*, 1992, 1994; Fan *et al.*, 1998). It is shown that when the discontinuity topography is taken into account, a more reasonable tomographic result can be obtained and the resulting 3-D velocity model would fit the data better. However, almost all of the previous global tomographic studies assumed the Moho, 410 and 660 km discontinuities to have a flat geometry or even ignore their existence (in such cases, the discontinuities are approximated by steep velocity gradients, e.g., Inoue *et al.* (1990)). Theoretically, the effect of the discontinuity topography can be evaluated when the block or grid is sufficiently smaller than the wavelength of the discontinuity undulations. The block size or grid spacing in most of the actual studies, however, are not small enough

due to the limited ray coverage and the sparse seismic networks. Hence the obtained tomographic images, especially those near discontinuities, represent not only velocity variations themselves, but also contain the effect of the discontinuity undulations (Zhao *et al.*, 1992, 1994).

Secondly, we have used a grid parameterization to express the Earth structure (Figure 2). Most of the previous global tomographic studies used blocks to express the Earth structure : the medium under study is divided into cubic blocks, seismic velocity in each of the blocks is assumed to be constant, and the velocity changes abruptly from block to block (Figure 2a). Thus, artificial velocity boundaries (discontinuities) are introduced into the model in both horizontal and vertical directions between blocks. In addition, the geometry of velocity anomalies is specified (to be blocks). Some studies even assumed ray paths within each block to be straight lines, which may be acceptable only when the block size is small. In global studies, however, the block size is not small enough because of the sparse distribution of seismic stations, particularly under oceanic regions. These problems do not exist or can be greatly alleviated when grid nodes are used to parameterize the Earth structure. For details, see the next section.

Thirdly, in this study we have used an efficient 3-D ray tracing technique to compute travel times and ray paths. So far, almost all of the global tomographic studies have used simple 1-D ray tracing methods. In very heterogeneous regions with high-velocity subducting slabs and low-velocity mantle plumes, ray trajectories calculated for a 1-D velocity model may deviate considerably from the real ones for long rays (Zhao *et al.*, 1992 ; Koketsu and Sekine, 1998). The final tomographic images would be distorted by this effect.

Applying our novel approach to the International Seismological Center (ISC) data sets reprocessed by Engdahl *et al.* (1998), we have determined a new 3-D P-wave velocity model of the whole mantle. Our results shed new light on the structure and dynamics of the Earth's deep interior, in particular, that of the subducting slabs and mantle plumes.

2. Method and Data

The methodology used in this work is a modified version of the tomographic method of Zhao *et al.* (1992, 1994) that is extended from the local/regional scale to a global scale. We first set up a 3-D grid net in the whole mantle. Velocity perturbations at the grid nodes from the starting one-dimensional (1-D) velocity model are taken as unknown parameters. The velocity perturbation at any point in the model is computed by linearly interpolating the velocity perturbations at the eight grid nodes surrounding that point. Thus in the grid model (Figure 2b), there are no artificial velocity boundaries as existing between blocks in the block models (Figure 2a).

We consider three seismic velocity boundaries, the Moho, 410 and 660 km discontinuities, in the mantle. In the tomographic inversion of the present work, we only take into account the depth variations of the 410 and 660 km discontinuities and used the results of Flanagan and Shearer (1998) (Figure 1). The Moho depth is taken to be 35 km,

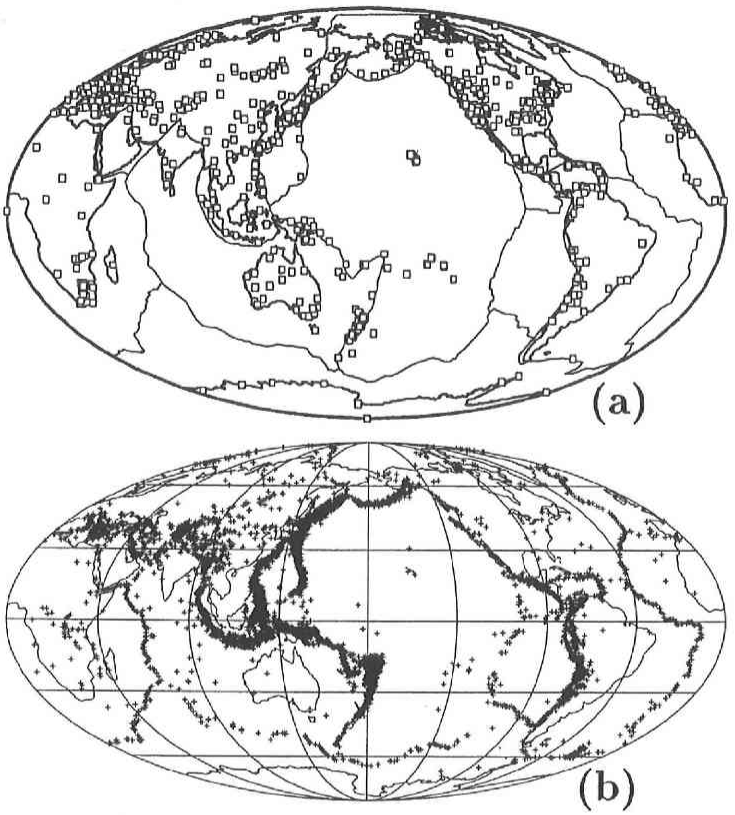

Fig. 3. (a) Distribution of the ISC seismic stations used in this study. (b) Hypocentral distribution of 7128 earthquakes used in this study. These events generated over 800,000 arrival times used in the tomographic inversions.

a value of the global average (Kennett and Engdahl, 1991 ; Mooney *et al.*, 1998). The Moho topography (Mooney *et al.*, 1998) will be taken into account in the next phase of the work. The geometries of the three discontinuities are fixed in the inversion process, and only the velocities at the grid nodes are determined. If sufficient later phase data, particularly those reflected and/or converted at the discontinuities, are available, the discontinuity geometries can also be determined together with the velocities at grid nodes. This will be the topic of a future study.

Ray paths and travel times are computed with an efficient 3-D ray tracing scheme (Zhao *et al.*, 1992) that is adaptable to a velocity model with complex velocity discontinuities and with 3-D velocity variations everywhere in the model. The principle of this ray tracing scheme is to use the pseudo-bending algorithm (Um and Thurber, 1987) and Snell' s law iteratively to perturb an initial ray estimate until a converged solution (the ray with the shortest traveltime) is found. Then we construct a system of observation equations that relate the observed travel times to hypocentral and velocity unknown parameters. To conduct inversions of the observation equations we used the LSQR algorithm (Paige

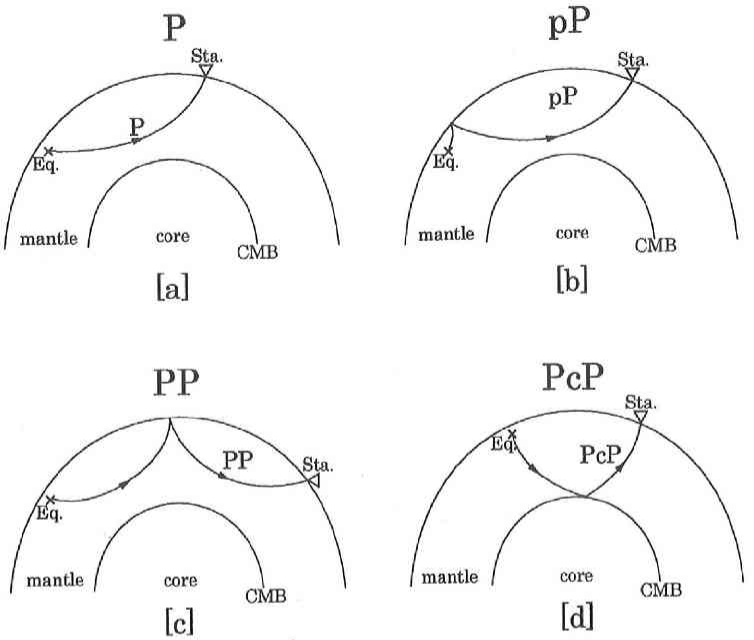

Fig. 4. Schematic illustrations of the seismic rays used in this study: (a) direct P waves, (b) depth phases pP waves, (c) surface reflected PP waves, and (d) core reflected PcP waves.

and Saunders, 1982) with damping and smoothing. Hypocenters are relocated in the inversion process.

We used the ISC travel time data during 1964 to 1998 reprocessed by Engdahl *et al.* (1998). Figure 3a shows the distribution of seismic stations compiled by ISC. We can see that the continental regions are generally well covered by the stations, while the oceanic regions are not. Figure 3b shows the distribution of 7128 earthquakes which are selected for this work. All of the 7128 events were recorded by over 50 stations and have errors in hypocentral locations less than 7 km. Their focal depths are well constrained by the use of depth phases (pP). In addition to first P arrivals, we also used three types of later phases in this study. They are the depth phases (pP), surface reflected waves (PP) and core reflected waves (PcP) (Figure 4). In total, we used approximately 800,000 arrival times in the tomographic inversions.

3. Analyses and Results

Before describing the major results of the mantle tomography, we first show the results of resolution analyses. We conducted the checkerboard resolution tests (Zhao *et al.*, 1992) to evaluate the adequacy of the ray coverage and spatial resolution. Figure 5 shows the results of the checkerboard test for representative layers in the mantle. In the preliminary analyses, we set up grid nodes in the whole mantle with a grid spacing

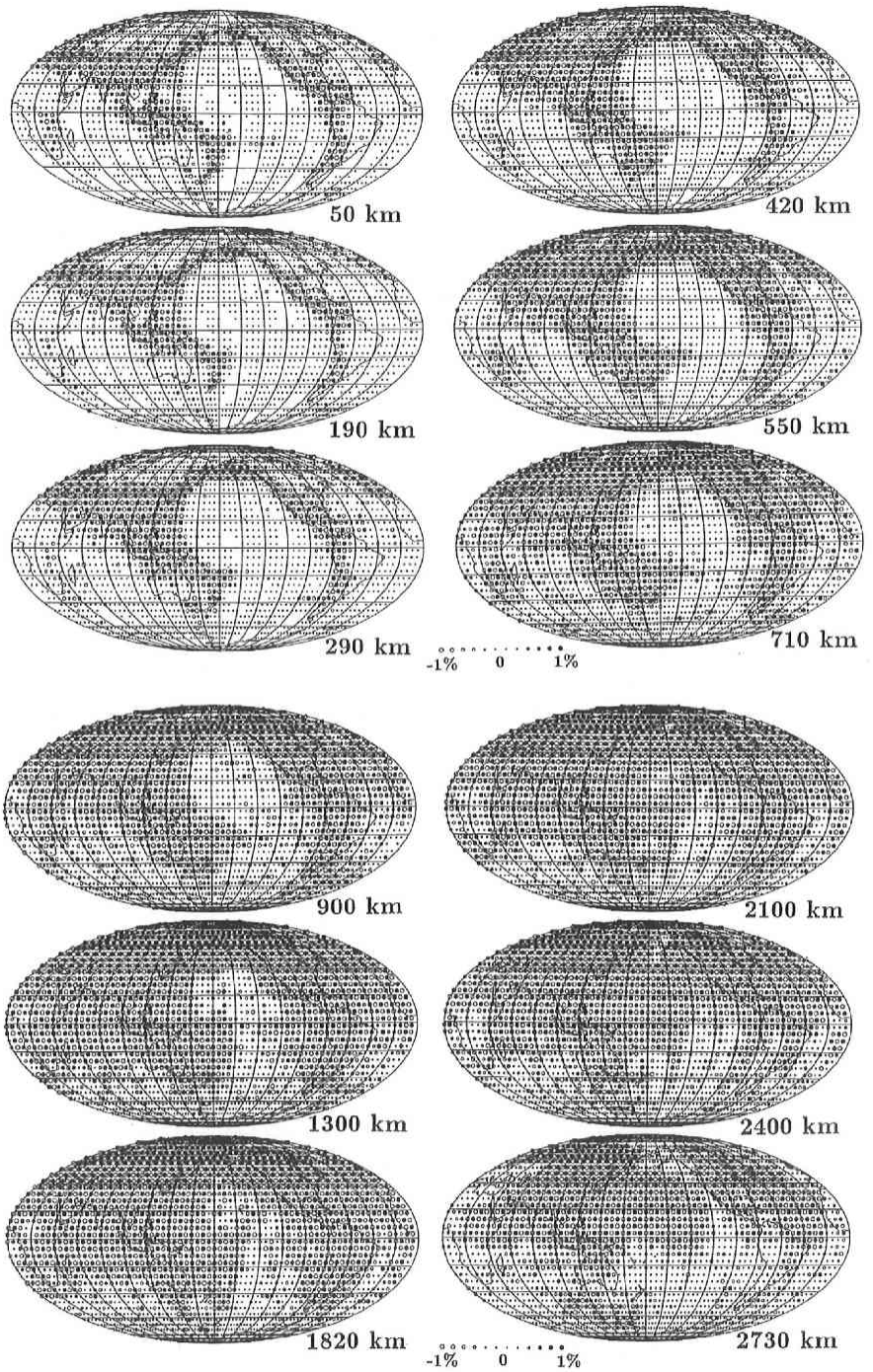

Fig. 5. Results of checkerboard resolution test for some representative depth slices in the mantle. Open and solid circles denote slow and fast velocities, respectively. The layer depth is shown below each map.

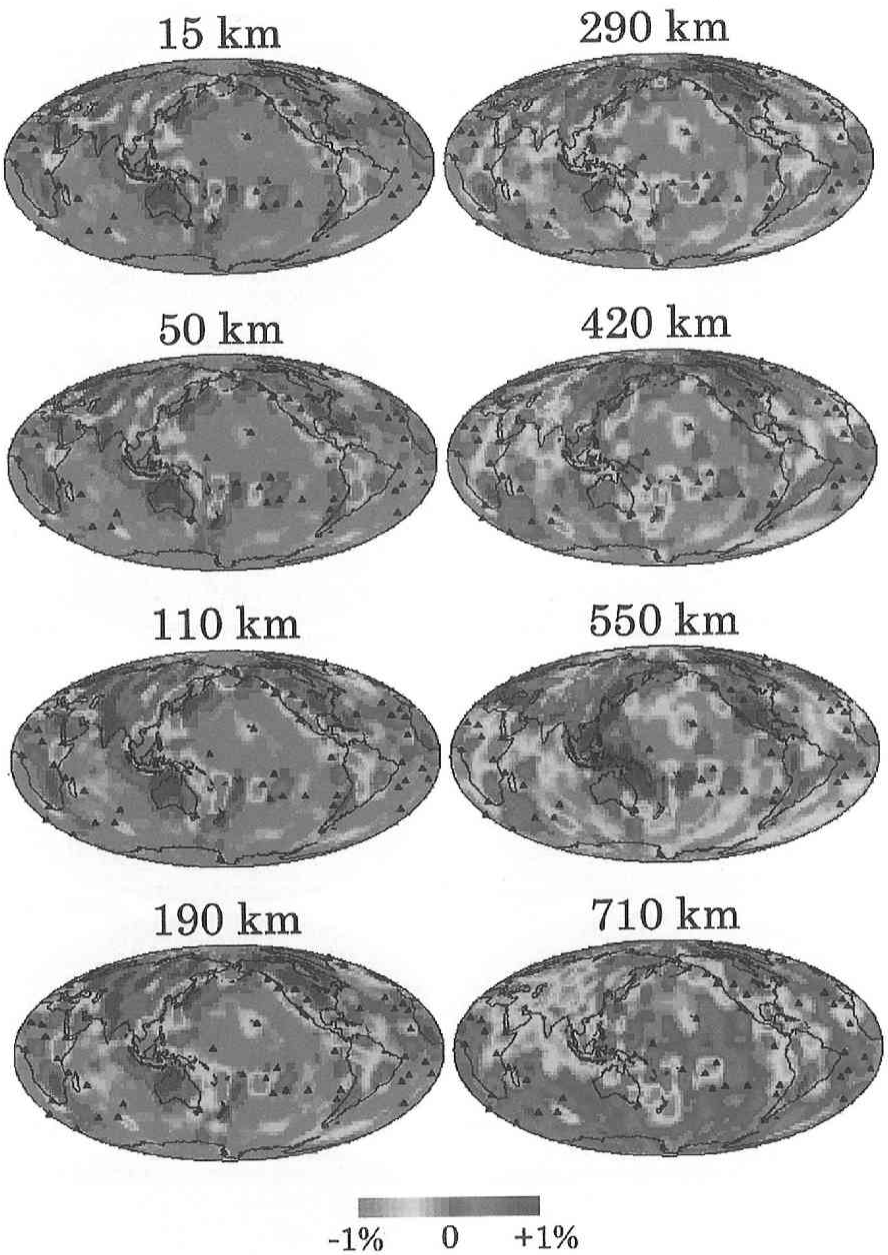

Fig. 6. P-wave velocity perturbations from the average velocity at each depth slice in the mantle. The depth of each layer is shown above each map. Red and blue colors denote slow and fast velocities, respectively. The velocity perturbation scale is shown at the bottom. Solid triangles denote the hotspots that appear on the Earth's surface.

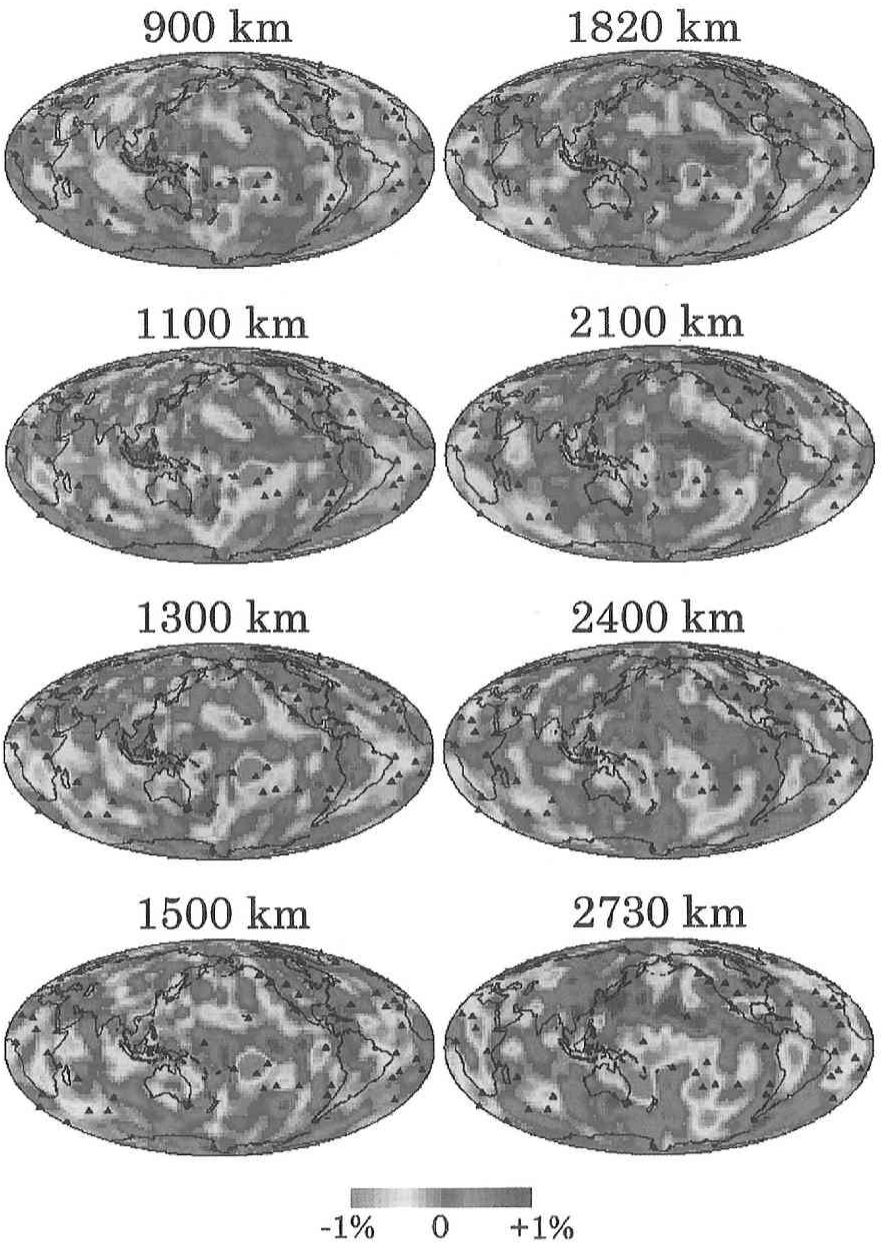

Figure 6 (Continue)

of five degrees laterally and 15 to 330 km in depth. The iasp91 Earth model (Kennett and Engdahl, 1991) is used as the starting velocity model for the 3-D inversions. We can see from Figure 5 that, in the upper mantle the resolution is good under the continental regions but poor under oceans. For the lower mantle, the spatial resolution is generally good for most of the mantle.

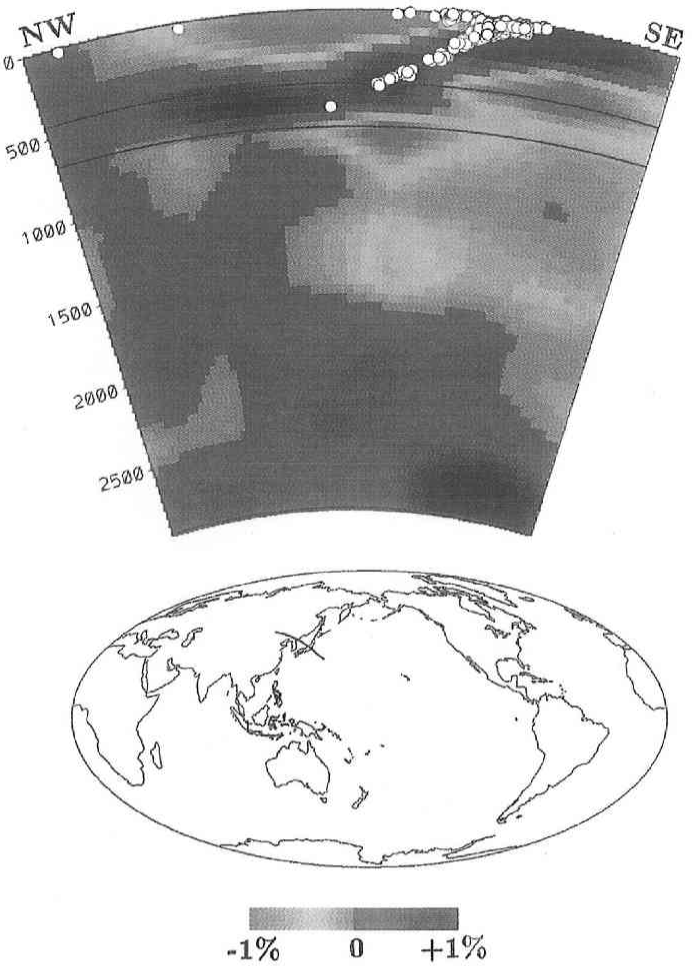

Fig. 7. Vertical cross section of P-wave velocity image along a profile passing through northeast China and central Japan. Location of the profile is shown on the world map. Red and blue colors denote slow and fast velocities, respectively. The velocity perturbation scale is shown at the bottom. White circles denote earthquakes that occurred within a 40-km width from the profile.

Figure 6 shows the P-wave tomographic images of the mantle obtained in this work. The velocity perturbations are from the average velocity at each depth. Locations of the 47 hotspots (Richards *et al.*, 1988) are also shown in the images. Figures 7-9 show some vertical cross sections of the tomographic images. For the upper mantle, our new model contains the general features observed in the previous models (e.g., Inoue *et al.*, 1990 ; Zhou, 1996 ; Bijwaard *et al.*, 1998) : a low-velocity ring around the Pacific Ocean basins and high-velocity anomalies under the old and stable continents in the depth range of 0-400 km. This suggests that the differences between continents and oceans persist down to about 400 km depth, above the mantle transition zone. Strong and wide high-

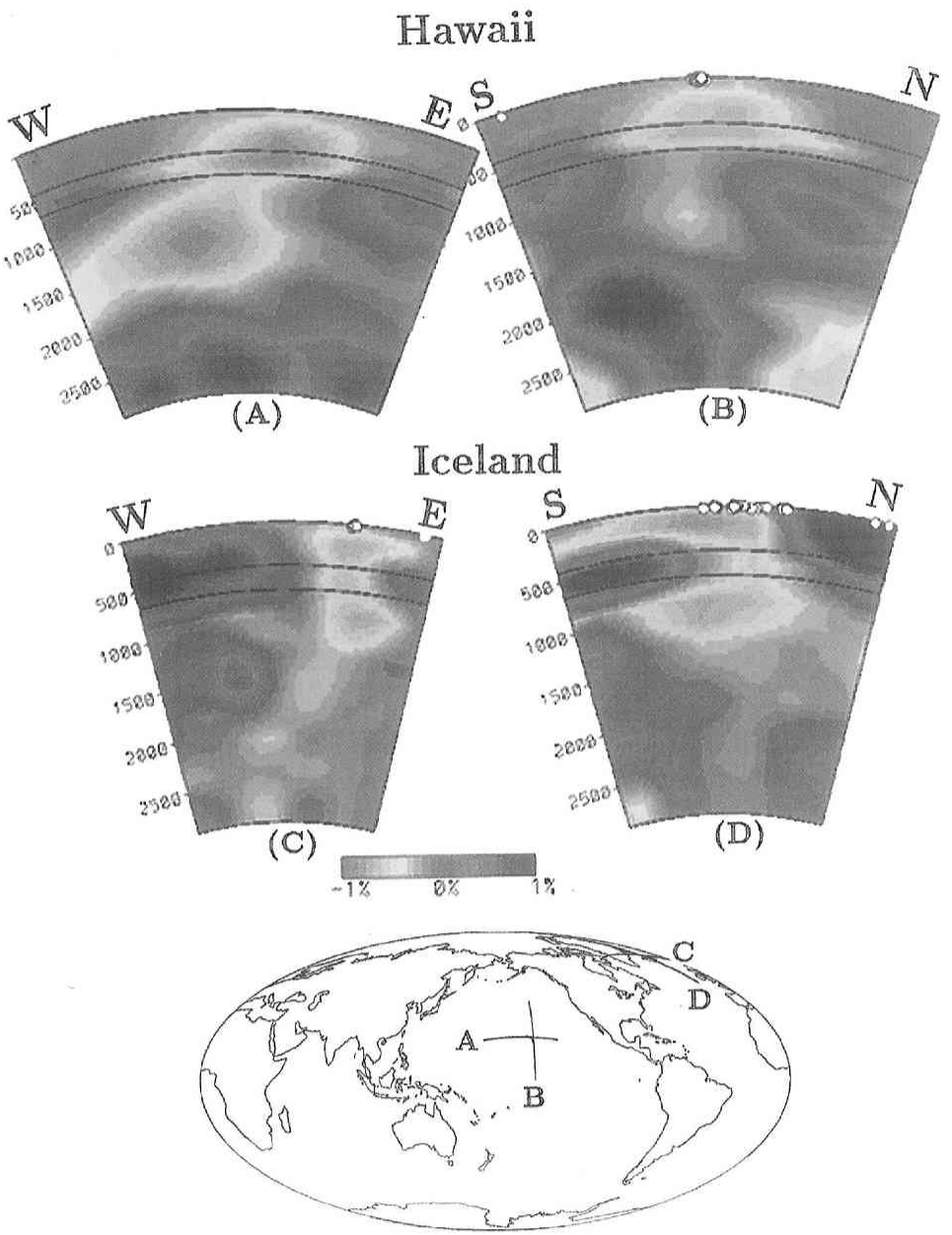

Fig. 8. (A) East-west and (B) north-south vertical cross sections of P-wave velocity images under Hawaii. (C) East-west and (D) north-south vertical cross sections of P-wave images under Iceland. Locations of the profiles are shown on the world map. Red and blue colors denote slow and fast velocities, respectively. The velocity perturbation scale is shown below the cross sections. Open circles denote earthquakes that occurred within a 40-km width from each of the profiles.

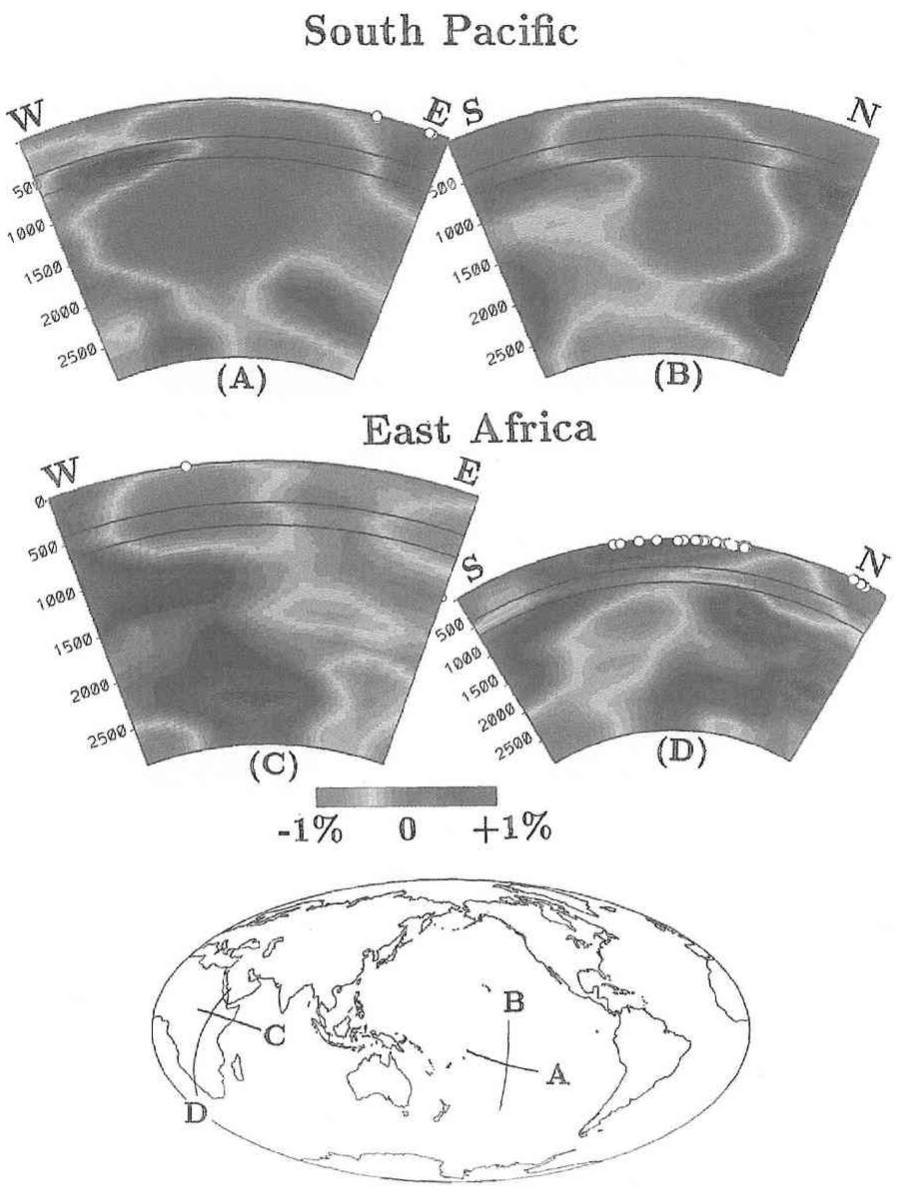

Fig. 9. (A and B) Vertical cross sections of P-wave velocity images under South Pacific. (C and D) Vertical cross sections of P-wave images under East Africa. Locations of the profiles are shown on the world map. Red and blue colors denote slow and fast velocities, respectively. The velocity perturbation scale is shown below the cross sections. Open circles denote earthquakes that occurred within a 40-km width from each of the profiles.

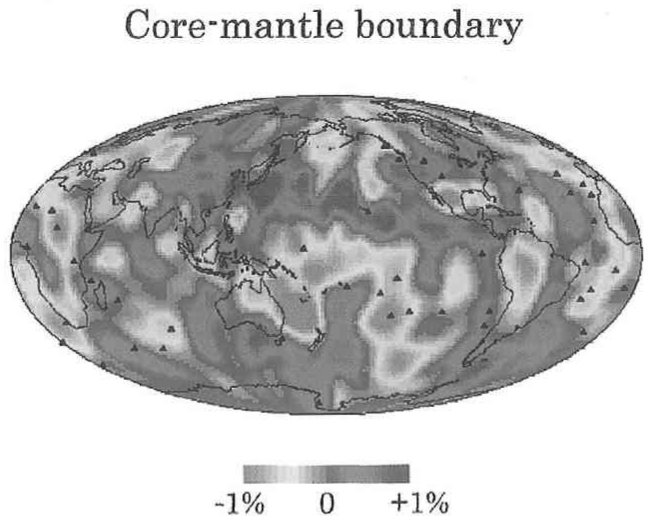

Fig. 10. P-wave velocity image at the base of the mantle. Red and blue colors denote slow and fast velocities, respectively. The velocity perturbation scale is shown at the bottom. Solid triangles denote the hotspots that appear on the Earth's surface. Note that there is a good correlation between the low-velocity zones and the distribution of hotspots.

velocity anomalies are visible in the transition zone under the subduction zone regions (see the image at 550 km depth), and moderately fast anomalies exist in the lower mantle under some of the subduction regions (Figures 6, 7). Prominent slow anomalies are visible under the hotspot regions in most parts of the mantle (Figures 8, 9). There is a good correlation between the distribution of hotspots on the surface and that of slow anomalies in the lower mantle down to the core-mantle boundary (CMB) (Figure 10). These features are discussed in details in the following section.

A unique feature of the present study is that we have taken into account the depth variations of the 410 and 660 km discontinuities (Flanagan and Shearer, 1998) (Figure 1) in the tomographic inversions. It would be interesting to see how much the discontinuity topography would influence the velocity tomography. For this we conducted an inversion with the same data set and method but assumed the 410 and 660 km discontinuities to be flat without depth variations. Their average depths (418.0 and 660.0 km) are used in this inversion according to Flanagan and Shearer (1998).

Figure 11 shows the comparison of the two inversion results. For clarity only the region adjacent to Australia is shown. We can see that the patterns of the two velocity images are quite consistent, but there are considerable differences in the amplitude of the velocity anomalies. For example, the amplitude of the slow anomaly at 710 km under northwest Australia is reduced by about 50% when the discontinuity topography is taken into account. Major changes of the velocity images appear at the transition zone depths and little in other depth levels. We conducted a number of such inversions by changing

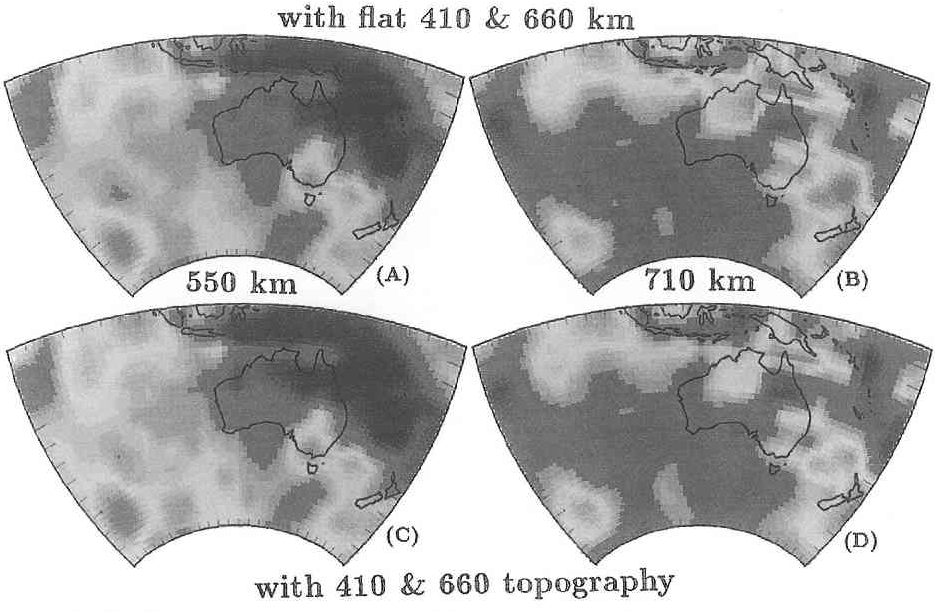

Fig. 11. P-wave velocity images at (a) 550 and (b) 710 km depths obtained by a tomographic inversion when the 410 and 660 km discontinuities are assumed to be flat. P-wave velocity images at (c) 550 and (d) 710 km depths when the 410 and 660 km discontinuities have depth variations as revealed by Flanagan and Shearer (1998). Red and blue colors denote slow and fast velocities, respectively. The velocity perturbation scale is the same as that in Figure 10. For clarity, only the region adjacent to Australia is shown.

the grid spacing, damping, smoothing and data sets. In general, the final travel time residual for the model including the discontinuity topography is reduced by 6-9% as compared to the model with flat discontinuities. This indicates that it is necessary to take into account the discontinuity topography in the tomographic inversions in order to image the detailed structure of the mantle.

4. Discussion and Conclusions

4.1. Deep structure of subduction zones

One distinct feature of the present model that differs from the previous ones is that stronger and wider high-velocity anomalies are visible in the transition zone depths under the subduction zone regions, and moderately fast anomalies exist in the lower mantle under those subduction regions (Figures 6, 7). This result may suggest that most of the slab materials are stagnant for a long time in the transition zone before finally dropping down to the lower mantle, and some of the slabs may only stay above the 660 km discontinuity and complete their convection within the upper mantle.

The subducting Pacific lithosphere under Japan is imaged clearly, and earthquakes occurred down to about 600 km depth within the slab (Figure 7). The thickness of the

slab looks like 150-200 km (Figure 7), which is caused by the lateral and vertical smearing of a thinner but stronger anomaly for the slab since we have used a relatively coarse grid. Our previous high-resolution studies using the local data sets have imaged the subducting Pacific slab as a high-velocity zone with a thickness of 90-100 km and a P-wave velocity 5-6% higher than the surrounding mantle (Zhao *et al.*, 1994, 1997). Low-velocity anomalies are visible on the back-arc side above the subducting Pacific slab (Figure 7), which is also consistent with the previous high-resolution results (Zhao *et al.*, 1994, 1997). The back-arc slow anomalies are generally considered to be associated with the arc and back-arc magmatism and volcanism caused by the dehydration process of the subducting slab and the convective circulation process of the mantle wedge (Zhao *et al.*, 1994, 1997).

An unexpected feature in Figure 7 is that prominent slow anomalies appear beneath the subducting Pacific slab and extend down to a depth of approximately 1600 km. This feature is also imaged by Fukao *et al.* (1992) and Zhao *et al.* (1994). It is unclear what the slow anomalies represent. There may be two possibilities: one is that they represent the hot upwelling portion of a local-scale convection associated with the subduction of the Pacific slab; the other is that they show a mantle plume rising from the lower mantle (Zhao *et al.*, 1994). Future detailed studies are needed to clarify this problem.

4.2. Hotspots and mantle plumes

Hotspots are regions of significant midplate volcanism, such as Hawaii, or very voluminous on-ridge volcanism, such as Iceland. Wilson (1963) first proposed that island chains like the Hawaiian-Emperor chain could be viewed as the tracks left on the moving plate by a fixed source beneath it. Morgan (1971) first suggested that the fixed source could in fact be partial melting of hot materials supplied by mantle plumes which are thin cylindrical upwellings of hot, low-viscosity material. Plume material ascends buoyantly from a basal thermal boundary layer (which might be either at the base of the mantle or at the base of the upper mantle) eventually interacting with the lithosphere at relatively shallow depths (Sleep, 1990, 1996). Nataf (1991) summarized the main properties of hotspots as follows: (1) The duration of most hotspots is at least 100 Ma; (2) Their relative moving velocities are generally much smaller than 1 cm/a; (3) Their spacing can be as low as 500 km; (4) They often tap "primitive" material, i.e., material that has never been processed in geochemical cycles at the surface; (5) They occur beneath oceans and continents; (6) They seem to be made of materials whose viscosity is several orders of magnitude lower than that of the surrounding mantle.

Hotspots have an irregular but nonrandom distribution over the Earth's surface. They are preferentially located near the divergent plate boundaries (mid-ocean ridges) and the long-wavelength geoid highs, and are preferentially excluded from regions near the convergent plate boundaries, in particular, subduction zones (Stefanick and Jurdy, 1984; Richards *et al.*, 1988; Weinstein and Olson, 1989). In addition, hotspots are generally located in slow velocity regions in the lower mantle (Hager *et al.*, 1985; Su *et al.*, 1994) and ultra-slow velocity patches on CMB (Williams *et al.*, 1998). Our present

tomographic images show that there is a good correlation between the distribution of hotspots on the surface and that of slow anomalies in the lower mantle down to the CMB (Figure 10). These results suggest that most of the large mantle plumes under the strong hotspots may originate from the CMB. However, there are a few hotspots that do not lie above the low-velocity regions over CMB (Figure 10). Those hotspots could be (a) associated with highly localized (and as yet undetected) low-V zones, (b) produced by lateral flow or deflection of plumes (Loper, 1991 ; Sleep, 1996 ; Steinberger, 2000), or (c) derived from a different depth or through a different process than the low-velocity associated hotspots (Anderson, 1975 ; Williams *et al.*, 1998). Albers and Christensen (1996) suggested that strong plumes (e.g., Hawaii) could originate at the CMB, however, weak plumes may not rise from CMB but from the transition zone depths if there is a thermal boundary layer there. Anderson (2000) suggested some upper mantle origins of hotspots instead of plumes in the lower mantle.

The slow anomalies under hotspots usually do not show a straight pillar shape, but exhibit winding images (Figures 8, 9). This suggests that plumes are not fixed in the mantle but can be deflected due to the influences of mantle convection, or mantle winds (e.g., Griffiths and Richards, 1989 ; Loper, 1991). Recent numerical experiments by Steinberger (2000) show that plume conduits can be tilted, with source regions at the D″ layer moving in the lowermost mantle flow, generally toward large-scale upwellings under southern Africa and the south central Pacific. Hotspot surface motion often represents the horizontal component of midmantle flow, which is frequently opposite to plate motion, toward ridges and away from subduction zones.

Under Hawaii, our tomography shows a tilted low-velocity zone in the entire mantle with one end right beneath the Hawaii Island and the other end located a few hundreds kilometers north of Hawaii at the CMB (Figures 6, 8b). Recently, Ji and Nataf (1998) used a diffraction tomography method to determine the lowermost mantle structure under Hawaii and found that a low-velocity zone exists over CMB north to northwest of Hawaii. Their result is generally compatible with ours considering the differences in the resolution scales of the two images.

Our plume images under Iceland show a vertical low-velocity zone in the entire mantle (Figures 8c, 8d), which are generally similar to the tomographic images determined recently by Bijwaard and Spakman (1999). The Iceland plume looks narrow in the east-west direction (Figure 8c), while it becomes wider in the north-south direction (Figure 8d). The low-V zone extends toward the south at depths shallower than about 400 km depth (Figure 8d). These features may be associated with the fact that the Iceland hotspot is located on the North Atlantic ridge which runs in the north-south direction. A part of the hot upwelling materials from the Iceland plume head may flow along the Reykjanes Ridge that is located south of Iceland, as shown by Sleep (1996) with numerical simulations. Recently, Foulger *et al.* (2000) conducted a high-resolution teleseismic tomography study to determine 3-D P and S wave velocity structures of the upper mantle under Iceland. Their results also show that the Iceland plume is narrow in the east-west direction and becomes wide in the north-south and extends toward the

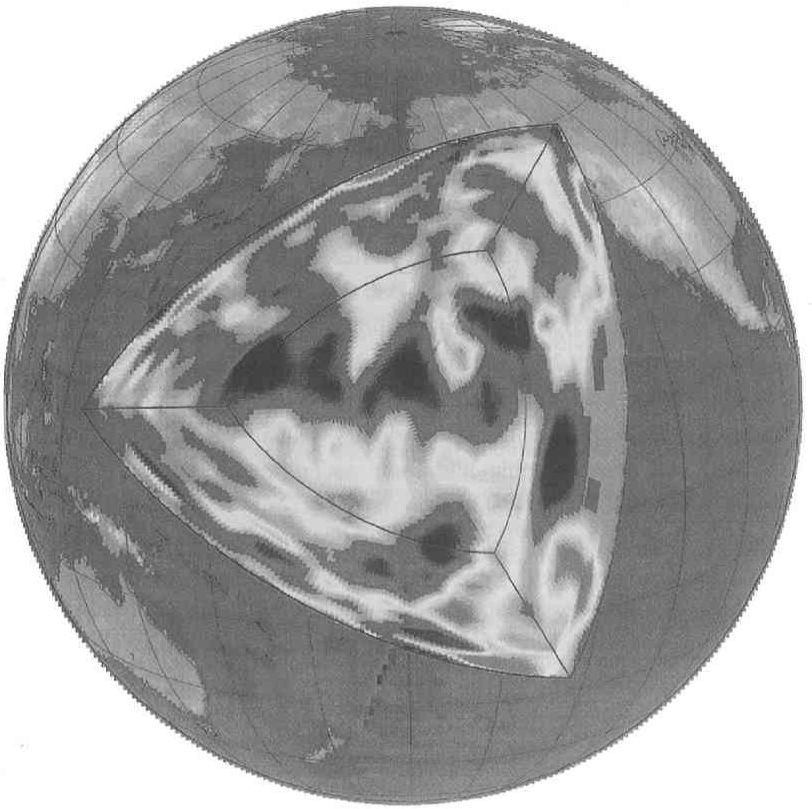

Fig. 12. Three-dimensional image of P wave velocity structure down to the core-mantle boundary (CMB) under the Pacific Ocean. The image within the central triangle shows velocity variations at the CMB. The surrounding three fans show the velocity images of the whole mantle along each vertical cross section. The remaining parts show the Earth's surface topography. Blue and red colors denote fast and slow velocities, respectively. The velocity perturbations are from −1% to +1% deviating from the average one-dimensional Earth model.

Reykjanes Ridge in the south, which is well consistent with our present results.

Under South Pacific and East Africa, huge low-velocity anomalies of over 1,000 km wide are visible in the whole mantle (Figure 9), which may show the images of super-plumes (McNutt and Fisher, 1987; Su *et al.*, 1994; Vinnik *et al.*, 1997; Ritsema *et al.*, 1999; Niu *et al.*, 2000; Nyblade *et al.*, 2000). Steinberger (2000) calculated the motion of hotspots in East Africa and the deformation of their underlying plume conduits with models of global mantle flow and suggested the presence of comparatively broad upwellings rather than localized plumes. This may explain the large and complex geometry of the low-velocity zones we imaged under East Africa.

As a consequence of the deflection of mantle plumes influenced by the mantle winds, hotspots would not be fixed in the geological history but could wander on the Earth's surface, as evidenced by the geomagnetic and numeric modeling studies, though their

relative moving velocities are much smaller than that of the lithospheric plates (Molnar and Stock, 1987; Griffiths and Richards, 1989; Steinberger, 2000).

Seismic velocity variations are affected by many factors, such as temperature, composition, partial melting, fluids, cracks, etc., but we still have no effective methods to discriminate between these contributions. If we assume that the slow velocities under the hotspot regions are entirely caused by high temperatures, we may use the method of Karato (1993) to estimate the excess temperatures of the plumes to be in the range of 200-300 K. This is compatible with the estimates from numerical experiments (Albers and Christensen, 1996; Steinberger, 2000). But the amplitudes of the velocity anomalies we obtained may be affected by the damping and smoothing in the inversion process, thus the excess temperatures may be also influenced.

Figure 12 shows a three-dimensional image of P-wave velocity structure down to the CMB under the Pacific Ocean. The velocity variations on the CMB, the plumes under the central and south Pacific and their ascending up to the Earth surface are visible.

The results presented in this article are still preliminary. In the next step of our global tomography work, we will take into account the depth variations of the Moho discontinuity (Mooney *et al.*, 1998), adopt a smaller and irregular grid to account for the nonuniform ray coverage, and use millions of data in the inversions. The plate tectonic and plume tectonic implications of the tomographic results will also be scrutinized in more details.

Acknowledgements: The author is grateful to E.R. Engdahl for providing his reprocessed ISC data sets. P. Shearer made available his model for the topography of the 410 and 660 km discontinuities. I thank Drs. A. Hasegawa, T. Inoue, T. Irifune, S. Maruyama, E. Ohtani, D. Suetsugu and E. Takahashi for thoughtful discussion. Prof. A. Hasegawa provided a constructive review that improved the manuscript. This work was partially supported by a grant (Kiban-B No. 11440134) from the Japanese Ministry of Education, Science and Culture (Monbusho).

References

Albers, M. and U. Christensen, 1996: The excess temperature of plumes rising from the core-mantle boundary, *Geophys. Res. Lett.*, **23**, 3567-3570.

Anderson, D., 1975: Chemical plumes in the mantle, *Geol. Soc. Am. Bull.*, **86**, 1593-1600.

Anderson, D., 2000: The thermal state of the upper mantle; No role for mantle plumes, *Geophys. Res. Lett.*, **27**, 3623-3626.

Bijwaard, H. and W. Spakman, 1999: Tomographic evidence for a narrow whole mantle plume below Iceland, *Earth Planet. Sci. Lett.*, **166**, 121-126.

Bijwaard, H., W. Spakman and E. Engdahl, 1998: Closing the gap between regional and global travel time tomography, *J. Geophys. Res.*, **103**, 30055-30078.

Boschi, L. and A. Dziewonski, 1999: High- and low-resolution images of the Earth's mantle: Implications of different approaches to tomographic modeling, *J. Geophys. Res.*, **104**, 25567-25594.

Dziewonski, A., 1984: Mapping the lower mantle: Determination of lateral heterogeneity in P

velocity up to degree and order 6, *J. Geophys. Res.*, **89**, 5929-5952.
Dziewonski, A. and D. Anderson, 1981 : Preliminary Reference Earth Model, *Phys. Earth Planet. Inter.*, **25**, 297-356.
Dziewonski, A., B. Hager and R. O'Connell, 1977 : Large-scale heterogeneities in the lower mantle, *J. Geophys. Res.*, **82**, 239-255.
Engdahl, E.R., R. van der Hilst and R.P. Buland, 1998 : Global teleseismic earthquake relocation with improved travel times and procedures for depth determination, *Bull. Seismol. Soc. Am.*, 88, 722-743.
Fan, G., T. Wallace and D. Zhao, 1998 : Tomographic imaging of deep velocity structure beneath the eastern and southern Carpathians, Romania : Implications for continental collision, *J. Geophys. Res.*, **103**, 2705-2723.
Flanagan, M. and P. Shearer, 1998 : Global mapping of topography on transition zone velocity discontinuities by stacking SS precursors, *J. Geophys. Res.*, **103**, 2673-2692.
Foulger, G., M. Pritchard, B. Julian and J. Evans, 2000 : The seismic anomaly beneath Iceland extends down to the mantle transition zone and no deeper, *Geophys. J. Int.*, 142, F1-F5.
Fukao, Y., M. Obayashi, H. Inoue and M. Nenbai, Subducting slabs stagnant in the mantle transition zone, *J. Geophys. Res.*, **97**, 4809-4822.
Griffiths, R. and M. Richards, 1989 : The adjustment of mantle plumes to changes in plate motion, *Geophys. Res. Lett.*, **16**, 437-440.
Hager, B., R. Clayton, M. Richards, R. Comer and A. Dziewonski, 1985 : Lower mantle heterogeneity, dynamic topography and the geoid, *Nature*, **313**, 541-545.
Inoue, H., Y. Fukao, K. Tanabe and Y. Ogata, 1990 : Whole mantle P wave travel time tomography, *Phys. Earth Planet. Inter.*, **59**, 294-328.
Ji, Y. and H. Nataf, 1998 : Detection of mantle plumes in the lower mantle by diffraction tomography : Hawaii, *Earth Planet. Sci. Lett.*, **159**, 99-115.
Karato, S., 1993 : Importance of anelasticity in the interpretation of seismic tomography, *Geophys. Res. Lett.*, **20**, 1623-1626.
Kennett, B. and E. Engdahl, 1991 : Traveltimes for global earthquake location and phase identification, *Geophys. J. Int.*, **105**, 429-465.
Kennett, B., E. Engdahl and R. Buland, 1995 : Constraints on seismic velocities in the Earth from traveltimes, *Geophys. J. Int.*, **122**, 108-124.
Koketsu, K. and S. Sekine, 1998 : Pseudo-bending method for three-dimensional seismic ray tracing in a spherical earth with discontinuities, *Geophys. J. Int.*, **132**, 339-346.
Loper, D., 1991 : Mantle plumes, *Tectonophysics*, **187**, 373-384.
McNutt, M. and K. Fischer, 1987 : The South Pacific superswell, in *Seamounts, Islands, and Atolls, Geophys. Monogr. Ser.*, Vol. 43, edited by B. Keating and R. Batiza, pp. 25-34, AGU, Washington, D.C.
Molnar, P. and J. Stock, 1987 : Relative motions of hotspots in the Pacific, Atlantic, and India oceans since late Cretaceous time, *Nature*, **327**, 587-591.
Mooney, W., G. Laske and T. Master, 1998 : CRUST 5.1 : A global crustal model at 5×5, *J. Geophys. Res.*, **103**, 727-747.
Morgan, W., 1971 : Convection plumes in the lower mantle, *Nature*, **230**, 42-43.
Nakanishi, I. and D. Anderson, 1982 : Worldwide distribution of group velocity of mantle Rayleigh waves as determined by spherical harmonic inversion, *Bull. Seismol. Soc. Am.*, **72**, 1185-1194.
Nataf, H., 1991 : Mantle convection, plates, and hotspots, *Tectonophysics*, **187**, 361-371.
Niu, F., H. Inoue, D. Suetsugu and K. Kanjo, 2000 : Seismic evidence for a thinner mantle transition zone beneath the South Pacific Superswell, *Geophys. Res. Lett.*, **27**, 1981-1984.
Nyblade, A., T. Owens, H. Gurrola, J. Ritsema and C. Langston, 2000 : Seismic evidence for a deep upper mantle thermal anomaly beneath east Africa, *Geology*, **28**, 599-602.
Paige, C. and M. Saunders, 1982 : LSQR : An algorithm for sparse linear equations and sparse least squares, *Assoc. Comput. Mach. Trans. Math. Software*, 8, 43-71.
Richards, M., B. Hager and N. Sleep, 1988 : Dynamically supported geoid highs over hotspots : Observation and theory, *J. Geophys. Res.*, **93**, 7690-7708.
Ritsema, J., H. Jan der Heijst and J. Woodhouse, 1999 : Complex shear wave velocity structure imaged beneath Africa and Iceland, *Science*, **286**, 1925-1928.

Sleep, N., 1990: Hotspots and mantle plumes: some phenomenology, *J. Geophys. Res.*, **95**, 6715-6736.

Sleep, N., 1996: Lateral flow of hot plume material ponded at sublithospherical depths, *J. Geophys. Res.*, **101**, 28065-28083.

Stefanick, M. and D. Jurdy, 1984: The distribution of hot spots, *J. Geophys. Res.*, **89**, 9919-9925.

Steinberger, B., 2000: Plumes in a convecting mantle: Models and observations for individual hotspots, *J. Geophys. Res.*, **105**, 11127-11152.

Su, W., R. Woodward and A. Dziewonski, 1994: Degree 12 model of shear velocity heterogeneity in the mantle, *J. Geophys. Res.*, **99**, 6945-6980.

Tanimoto, T., 1990: Long-wavelength S-wave velocity structure throughout the mantle, *Geophys. J. Int.*, **100**, 327-336.

Um, J. and C. Thurber, 1987: A fast algorithm for two-point seismic ray tracing, *Bull. Seism. Soc. Am.*, **77**, 972-986.

Vasco, D., L. Johnson and R. Pulliam, 1995: Lateral variations in mantle velocity structure and discontinuities determined from P, PP, S, SS, and SS-SdS travel time residuals, *J. Geophys. Res.*, **100**, 24037-24059.

Vinnik, L., S. Chevrot and J. Montagner, 1997: Evidence for a stagnant plume in the transition zone?, *Geophys. Res. Lett.*, **24**, 1007-1010.

Weinstein, S. and P. Olson, 1989: The proximity of hotspots to convergent and divergent plate boundaries, *Geophys. Res. Lett.*, **16**, 433-436.

Williams, Q., J. Revenaugh and E. Garnero, 1998: A correlation between ultra-low basal velocities in the mantle and hot spots, *Science*, **281**, 546-549.

Wilson, J., 1963: A possible origin of the Hawaiian islands, *Can. J. Phys.*, **41**, 863-870.

Woodhouse, J. and A. Dziewonski, 1984: Mapping the upper mantle: Three-dimensional modeling of Earth structure by inversion of seismic waveforms, *J. Geophys. Res.*, **89**, 5953-5986.

Zhang, Y. and T. Tanimoto, 1993: High-resolution global upper mantle structure and plate tectonics, *J. Geophys. Res.*, **98**, 9793-9823.

Zhao, D., A. Hasegawa and S. Horiuchi, 1992: Tomographic Imaging of P and S wave velocity structure beneath northeastern Japan, *J. Geophys. Res.*, **97**, 19909-19928.

Zhao, D., A. Hasegawa and H. Kanamori, 1994: Deep structure of Japan subduction zone as derived from local, regional and teleseismic events, *J. Geophys. Res.*, **99**, 22313-22329.

Zhao, D., Y. Xu, D. Wiens, L. Dorman, J. Hildebrand and S. Webb, 1997: Depth extent of the Lau back-arc spreading center and its relation to subduction processes, *Science*, **278**, 254-257.

Zhou, H., 1996: A high-resolution P wave model for the top 1,200 km of the mantle, *J. Geophys. Res.*, **101**, 27791-27810.